Journal of Biomedical Optics

SPIEDigitalLibrary.org/jbo

Diffuse near-infrared reflectance spectroscopy during heatstroke in a mouse model: pilot study

David Abookasis
Elad Zafrir
Elimelech Nesher
Albert Pinhasov
Shmuel Sternklar
Marlon S. Mathews

SPIE

Diffuse near-infrared reflectance spectroscopy during heatstroke in a mouse model: pilot study

David Abookasis,[a] Elad Zafrir,[a] Elimelech Nesher,[b] Albert Pinhasov,[b] Shmuel Sternklar,[a] and Marlon S. Mathews[c]
[a]Ariel University Center of Samaria, Department of Electrical and Electronic Engineering, Ariel 44837, Israel
[b]Ariel University Center of Samaria, Department of Molecular Biology, Ariel 44837, Israel
[c]University of California Irvine, Department of Neurological Surgery, Medical Center, 101 The City Drive South, Orange, California 92868.

Abstract. Heatstroke, a form of hyperthermia, is a life-threatening condition characterized by an elevated core body temperature that rises above 40°C (104°F) and central nervous system dysfunction that results in delirium, convulsions, or coma. Without emergency treatment, the victim lapses into a coma and death soon follows. The study presented was conducted with a diffuse reflectance spectroscopy (DRS) setup to assess the effects of brain dysfunction that occurred during heatstroke in mice model ($n = 6$). It was hypothesized that DRS can be utilized in small animal studies to monitor change in internal brain tissue temperature during heatstroke injury since it induces a sequence of pathologic changes that change the tissue composition and structure. Heatstroke was induced by exposure of the mice body under general anesthesia, to a high ambient temperature. A type of DRS in which the brain tissue was illuminated through the intact scalp with a broadband light source and diffuse reflected spectra was employed, taking in the spectral region between 650 and 1000 nm and acquired at an angle of 90 deg at a position on the scalp ~12 mm from the illumination site. The temperature at the onset of the experiment was ~34°C (rectal temperature) with increasing intervals of 1°C until mouse death. The increase in temperature caused optical scattering signal changes consistent with a structural alteration of brain tissue, ultimately resulting in death. We have found that the peak absorbance intensity and its second derivative at specific wavelengths correlate well with temperature with an exponential dependence. Based on these findings, in order to estimate the influence of temperature on the internal brain tissue a reflectance-temperature index was established and was seen to correlate as well with measured temperature. Overall, results indicate variations in neural tissue properties during heatstroke and the feasibility to monitor and assess internal temperature variations using DRS. Although several approaches have described the rise in temperature and its impact on tissue, to the best of our knowledge no information is available describing the ability to monitor temperature during heatstroke with DRS. The motivation of this study was to successfully describe this ability. [DOI: 10.1117/1.JBO.17.10.105009]

Keywords: heatstroke; diffuse reflectance; optical properties; absorbance; cerebral hemodynamics.

Paper 12253 received Apr. 24, 2012; revised manuscript received Sep. 12, 2012; accepted for publication Sep. 20, 2012; published online Oct. 18, 2012; corrected Nov. 5, 2012.

1 Introduction

Systemic hyperthermia in the body is manifested as three separate entities: heat cramps, heat exhaustion and heatstroke, the latter two being life-threatening.[1–3] Signs of systemic hyperthermia include muscle cramps; excessive fatigue or weakness, or both; loss of coordination; a slowing of reaction time; headache; decrease comprehension; nausea and vomiting; and dizziness. Unlike heat cramps and heat exhaustion, heatstroke is a true medical emergency and is often fatal if not properly and promptly treated.[4–6] Heat stroke occurs particularly in non-acclimated individuals who are exposed to high environmental temperatures. The body normally generates heat as a result of metabolism, and the body is usually able to dissipate the heat by either radiation of heat through the skin or by evaporation of sweat. However, in extreme heat the thermal regulatory mechanisms fail, and body temperature rises. Usually, above 40°C (104°F) brain damage occurs and death follows if vigorous measures are not instituted.[7,8] Thus, early diagnosis and proper treatment are crucial for the patient's survival. Immediate cooling and support of organ-system function are the two main therapeutic objectives in patients with heatstroke. Several cooling methods have been presented in the literature including immersion in water at different temperatures, evaporative cooling, ice pack application, pharmacological treatment and invasive techniques.[9–11] The populations most susceptible to heatstrokes are infants, older people in poor health (often with associated heart diseases, lung diseases, kidney diseases, or on certain medications that make them vulnerable to heat strokes), athletes, or outdoor workers physically exerting themselves under the sun. Susceptibility is greater in those with a disorder of the skin or sweat glands, and those taking anticholinergic drugs (which reduce sweating). Overstrenuous activity, unsuitable clothing, overeating, and drinking too much alcohol are sometimes contributory factors. However, some individuals can develop symptoms of heatstroke suddenly and rapidly without warning.

It is widely accepted that heatstroke develops as a result of an increase in body temperature leading to multiorgan damage. Therefore, methods to monitor and measure changes in internal temperature are important. Current clinical methods for

Address all correspondence to: David Abookasis, Ariel University Center of Samaria, Department of Electrical and Electronic Engineering, Ariel 44837, Israel. Tel: 972-3-9066357; Fax: 972-3-9755807; E-mail: davida@ariel.ac.il

0091-3286/2012/$25.00 © 2012 SPIE

monitoring temperature are divided into two categories, invasive and noninvasive. Techniques such as tympanic membrane thermometry, zero heat flow, microwave radiometry, magnetic resonance thermometry, and ultrasound thermometry besides the conventional oral or rectal electronic thermometers are in use.[12,13] However, accuracy, complexity, cost, portability, safety, and continuous measurements can influence the suitability of these techniques. For instance, rectal temperature may not accurately reflect brain temperature, especially during global ischemia. The development of a non-invasive device which overcomes these factors will be vital in medical management of heatstroke. Interest in using optical techniques is on the rise as they possess many advantages such as being noninvasive, portable, relative low cost, easy to maintain, can be used repeatedly over a prolonged period of time with no adverse effects, and offer both high spatial and temporal resolution.[14–16] So far, several researchers have successfully demonstrated the feasibility of using optical techniques such as near-infrared spectroscopy[12,17–19] optical coherence tomography,[20] laser speckle imaging,[21] and fiber-optics sensors[22] to monitor temperature changes in a noninvasive fashion from turbid media as well as from living tissue.

Diffuse reflectance spectroscopy (DRS) is an established tool widely studied and used to investigate physiology below tissue surface. It is a simple, low-cost, and noninvasive modality with great potential for diagnostic applications as it is sensitive to absorption and scattering properties of biological molecules in tissue. Therefore, it has the potential to provide biochemical composition (chromophores content) and morphology (structure) information about biological tissue.[23–28] The spectroscopy of tissue is possible owing to the weak absorption of the tissue in the near infrared (NIR) window (650 to 1000 nm). Classical DRS platforms include a light source, detector (spectrograph), and a pair of optical fibers separated by a fixed distance for delivery (illuminating fiber) and collection (collecting fiber) of light during measurements. Light entering the tissue undergoes a combination of multiple scattering and absorption and the reflected light from the tissue, called diffuse reflectance (R_d), is recorded by the detector fiber. The light intensity decreases during its 'banana path' propagation according to the concentration of the absorbing chromophores (hemoglobin, fat, and water).[29–31] It has been shown that separation between the source and the detection points determines the sensitivity of the measured reflectance to the absorption coefficient (large separation distances, $> \sim 10$ mm) and to the scattering coefficient (short separation, $< \sim 1$ mm).[32–39] Optical properties (absorption and scattering) can be extracted from the captured radiation with analytical models or Monte Carlo simulations. Even though there are several ways to model the measured diffuse reflectance spectra, in this work we used the two-source diffusion-based model for tissue reflectance as described by Farrel et al.[40] The use of diffusion theory is applicable here since: 1. measurements are obtained far from the boundaries, 2. the source-detector separation is ~12 mm, and 3. the absorption effects in brain tissue are less than the scattering (the brain medium is very diffuse).

As mentioned, several research groups have used NIR spectroscopy techniques to study the influence of temperature on NIR spectra since both photon path length and refractive indices are temperature dependent and because of the strong temperature-sensitivity of water absorption, which is reflected in intensity changes and wavelength shifts around its peak at 970 nm.[18,41–44] In addition, the effects of temperature on major tissue absorbers such as hemoglobin and water have been studied elsewhere.[45,46] Works were obtained also to measure glucose under temperature perturbation.[47–50] The aim of this study is to continue exploring this possibility in the wavelength range from 650 to 1000 nm during heatstroke with a different approach and configuration. We point out three differences as compared to the other techniques. First, we focus here on the temperature dependence of the absorbance spectra shift and its second derivative characteristics at specific wavelengths to evaluate the internal temperature of brain tissue. Second, in our setup the source and detector are orthogonal to each other on a curved brain surface with ~12 mm separation. Finally, we assume that during changes in temperature there are changes in tissue concentrations such as hemoglobin and water. These molecules absorb specific wavelengths of light which alters the optical properties of tissue and consequentially alter the shape of the diffuse optical spectra. Therefore, we hypothesize that DRS can be used to monitor change in internal brain tissue temperature during heatstroke injury.

2 Materials and Methods

2.1 *Animal Preparation*

The study protocol described below was reviewed and approved by the *Institutional Animal Care and Use Committee* at *Ariel University Center*. Adult male mice (Sabra, aged eight to ten weeks, weight 45 to 50 g) were anesthetized by an intraperitoneal (IP) injection of combination of ketamine (100 mg/kg) and xylazine (16 mg/kg). The depth of anesthesia was ascertained by pinching of the toes or tail and by monitoring rate of breathing. Head was fixed and the hair was removed using hair removal cream. A folded heating plate (Thermo plate, Tokai Hit) was placed under the mouse to control the body temperature and a thermocouple rectal probe (YSI) was inserted ~2 cm to measure core body temperature. Hereafter, the temperature discussed is in reference to the measurements provided by the YSI probe. The mouse body was wrapped with aluminum foil to keep body temperature at a desired level. In live animals, heat is rapidly distributed throughout the body by circulating blood maintaining a uniform core body temperature. Thus a temperature gradient is not a concern for this experimental setup. A heating pad is widely used in rodent experiments to maintain a physiologic core body temperature during anesthesia. Heatstroke could be induced by viral or bacterial toxins, drugs (amphetamines, atropine, calcium antagonists, etc.), exercise, or exposure to a hot environment. As mentioned above, we choose the current model because of its simplicity and its popularity among research groups. Future research will consider changing this model and animal study. Other physiological parameters such as heart rate, and SpO_2 (arterial oxygen saturation) were monitored simultaneously using pulse oximeter (Nonin, 8650). All mice were kept in their habitual environment until the day of the experiment. Heatstroke was induced by increasing the temperature of the folded heating plate (available up to 50°C). Baseline reflectance measurements were obtained for 10 min prior to external induction of hyperthermia. Thus each mouse served as its own control, decreasing the number of animals required for the study. All mice ($n = 6$) underwent the same procedure. The measurements were started from baseline body temperature with increases of 1°C in interval times of ~3 min between measurements until mouse death. Table 1

Table 1 Mice details during experiments. The standard error represents combinations of variations in experimental conditions as well as differences in individual mice.

	Mouse1	Mouse2	Mouse3	Mouse4	Mouse5	Mouse6	Mean ± SE
Age (weeks)	10	9	11	8	10	9	9.5 ± 0.51
Weight (g)	45	45	48	48	46	48	46.4 ± 0.68
Baseline temperature (°C)	32	34	33	34	38	32	33.8 ± 1.01
Heatstroke (°C)	40	39	38	40	43	39	39.8 ± 0.83

presents the experimental details per mouse. As can be seen, heatstroke (death) occurred at an average temperature of 40°C. This is lower than the conventional heatstroke level found in other mammals (~42°C) such as rats, dogs, rabbits[51] and is likely due to the small body feature of the individual mouse. The environmental temperature was measured continuously during the experiments with an liquid crystal display (LCD) digital thermometer (Extech Instrument) and was 23 ± 1°C.

2.2 *Instrumentation*

A schematic diagram of the setup is drawn schematically in Fig. 1. The setup consists of a wideband light source, two optical fibers, spectrometer, temperature controller, pulse oximeter, rectal probe, and a computer station with control software. The lamp inside the light source (Stockler & Yale, Inc., M1000) was replaced with a broadband quartz-tungsten-halogen (EIKO, EXR) to gives a smooth broadband spectral profile along the NIR region and stable intensity over time. One of the optical fibers (illuminating fiber) is connected to this light source with a diameter of $D = 5$ mm. The light emanating from the brain is delivered to the spectrometer (Stellarnet, EPP2000) via the second optical fiber (collecting fiber, $D = 2$ mm) positioned perpendicular to the first fiber; That is, the diffuse reflectance was collected by the second fiber-optic probe that was mounted on the surface of the mice scalp at 90° to the brain surface and connected to a spectrometer (see Fig. 1).

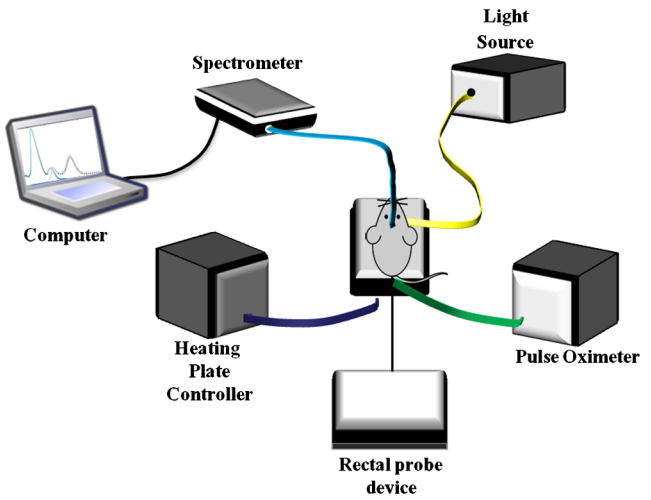

Fig. 1 Schematic configuration of the experimental apparatus. Light exiting the skull is collected by the collecting fiber mounted at an angle of 90 deg with respect to the incident beam. Source-detector separation (arc length) is ~12 mm.

In this configuration, the reflected light collected by the collection fiber propagates through the brain layers (scalp, skull, CSF, gray, and white matter). But at our source detector separation the dominant signal is from photons passing through the brain. Hence the detected signal is sensitive to changes in optical property from the brain. The reflected signal is then dispersed and detected by the charge coupled device (CCD) array in the spectrometer. The spectrometer system has a 2048-elements linear CCD array with 12-bit resolution, and with a spectral range from 240 to 1200 nm. The spectrometer was controlled by a laptop computer running Windows operating system and is connected to the USB port of the computer. Spectrometer interface software was used between the spectrometer and the computer to display the optical reflectance in real-time. Both fibers were connected to a mechanical stage translation for position control and care was taken to ensure full contact between the probes and the brain surface throughout the experiments.

2.3 *Calibration*

The measured diffuse reflectance spectra were normalized to remove the effects of the light source spectrum, fiber attenuation, and the detector response by using the relation;

$$\hat{R}_d(\lambda) = \frac{R_{d_{\mathrm{msr}}}(\lambda) - R_{\mathrm{dark}}(\lambda)}{R_{\mathrm{whiteSTD}}(\lambda) - R_{\mathrm{dark}}(\lambda)}, \tag{1}$$

where $\hat{R}_d$ is the normalized diffuse reflectance, $R_{d_{\mathrm{msr}}}$ measured diffuse reflectance (raw spectra), R_{whiteSTD} is the reflectance of a white standard, and R_{dark} is the reflectance acquired in complete darkness, so that it is due to the electrical noise (thermal noise) of the CCD array. The spectrometer is programmed to automatically subtract a background reading for every reflectance measurement. The white surface provided ~100% reflectance and was used to compensate for the spectral shape of the light emitted by the lamp and the wavelength-dependent sensitivity of the detector and the optics in the detecting system. Calibration spectra were routinely measured before data acquisition of the brain by placing the probe at a fixed distance from the white standard. It is quite usual and convenient to present the results in terms of absorbance (signal strength) spectra; A_s. Absorbance was calculated by taking the log of the normalized diffuse reflectance $\hat{R}_d$ defined as,

$$A_s(\lambda) = -\log_{10}\hat{R}_d(\lambda). \tag{2}$$

It is assumed that changes in spectral response are related to concentration as described by Beer's law;[52] the absorbance of an analyte is equivalent to the product of the molar absorptivity (ε) of a specific type of molecular vibration (referred also as a molar

extinction), the concentration (C) of the molecules in the measurement beam and the pathlength (d) of the sample. This relationship is most often expressed as: $A_s = \varepsilon \cdot C \cdot d$.

2.4 *Reflectance Model*

Numerous models based on the diffusion approximation of the transport equation have been described in the literature over the past few years.[53–58] In this study, we utilize the two-source diffusion theory model derived by Farrell et al.,[40] who calculate the diffuse reflectance $R(\rho)$ on the surface of a semi-infinite turbid medium in the diffusion approximation, i.e., &micro$_a \ll \mu_s'$ and ii) $\rho \gg (\mu_a + \mu_s')^{-1}$. Under these conditions, they obtained the following expression:

$$R_d(\rho) = \frac{k_1}{(\mu_a + \mu_s')}\left\{\left[\mu_{\text{eff}} + \frac{1}{r_1}\right]\cdot\frac{e^{-\mu_{\text{eff}}\cdot r_1}}{r_1^2} + \left(1 + \frac{4}{3}k_2\right)\left[\mu_{\text{eff}} + \frac{1}{r_2}\right]\cdot\frac{e^{-\mu_{\text{eff}}\cdot r_2}}{r_2^2}\right\}, \tag{3}$$

with

$$\mu_{\text{eff}} = \sqrt{3\mu_a(\mu_a + \mu_s')}, \quad r_1 = \sqrt{\rho^2 + \left(\frac{1}{\mu_a + \mu_s'}\right)^2},$$

$$r_2 = \sqrt{\rho^2 + \left[\frac{\left(1 + \frac{4}{3}k_2\right)}{\mu_a + \mu_s'}\right]^2},$$

where ρ - source-detector separation, μ_a- the absorption coefficient [1/mm], μ_s'- the reduced scattering coefficient [1/mm], μ_{eff} is the effective attenuation coefficient obtained from the other two optical coefficients, and k_1 and k_2 are related to the light source intensity and the refractive index of the medium, respectively. Variations in physiological conditions as a result of heatstroke lead to changes of the optical properties since they are temperature dependent, and hence to changes in R_d. For the given geometry shown in Fig. 1 and fixed source-detector separation, we use a tissue-like phantom with known optical properties over the wavelength range of 600 to 1000 nm to determine the values of k_1 and k_2 through the measured diffuse reflectance. A nonlinear least-squares fit with the Levenberg-Marquardt algorithm on Eq. (3) was performed and found $k_1 = 2000$ and $k_2 = 1.3$. Once the model [Eq. (3)] is calibrated against the experimental reflectance [Eq. (1)], it can be applied in an inverse manner to recover tissue optical properties. This will be demonstrated in the end of the next section.

2.5 *Data Analysis*

Prior to data analysis, the collected diffuse reflectance spectra, $\hat{R}_d$, was preprocessed using the *fspecial* function in MatLab to: 1. remove spectral artifacts such as pulsations of the cortex due to respiration and heartbeat, and 2. to eliminate high frequency noise originated from the spectrometer. All spectra for a given temperature were collected sequentially during single data collection session. Data analysis was performed off-line using in-house scripts written in MatLab. The spectral range of the processed spectra was in the range of 650 to 1000 nm with 2-nm increments. Spectra derivatives conducted during this study were performed using the *Savitzky-Golay* algorithm with respect to wavelength. Common statistics metrics such as Pearson's correlation coefficient (R), root mean squared error (RMSE), and mean relative error (MRE), were computed to assess the fitting ability between reference temperature and the predicted data. These metrics were calculated based on the following expressions:

$$R = \left[\frac{\sum_{i=1}^{n}(y_{i,\text{pred}} - \bar{y})^2}{\sum_{i=1}^{n}(y_{i,\text{ref}} - \bar{y})^2}\right]^{1/2} \tag{4}$$

$$\text{RMSE} = \sqrt{\frac{\sum_{i=1}^{n}(y_{i,\text{pred}} - y_{i,\text{ref}})^2}{n}}$$

$$\text{MRE} = \left\{\frac{1}{n}\sum_{i=1}^{n}\left|\frac{y_{i,\text{pred}} - y_{i,\text{ref}}}{y_{i,\text{ref}}}\right|\right\} \times 100.$$

In these equations, $y_{i,\text{ref}}$ is the reference (actual) temperature value at the i measurements obtained with the YSI probe, $y_{i,\text{pred}}$ represent the predicted (estimated) temperature by the developed RTI index, $\bar{y}$ is the mean of each measurement, and n is the total number of measurements used. We will use these metrics to evaluate the feasibility of temperature prediction on a new mice brain as part of the validation processing. All computations for this study were implemented with software written in MatLab platform (MathWorks, R2010b).

3 Results and Discussion

Figure 2(a) shows the absorbance spectrum measured on a representative mouse brain (mouse #1, Table 1) with three different temperatures (32°C, 38°C, and 40°C) out of 10 measurements, conducted on the same animal, for easier visual representation. In Fig. 2(b) the region between 940 and 1000 nm was magnified to emphasize the change in absorbance intensity peak around 970 nm. In both panels, the effect of temperature on the absorbance spectrum is clearly observed and the difference between spectral intensities is noticeable. Based on the effect of temperature on the absorbance measurements shown we assume that both scattering and absorption alterations occur as a result of chromophores and morphological changes. The dominant feature is in the absorbance of water that peaks around 970 nm. As it can be seen, this peak decreased and shifts slightly to a shorter wavelengths (left shift) as temperature rises. This shift to a lower wavelength as the temperature increases resemble the Wien's displacement law.[59] The intensity and shift changes at 970 nm are attributed to the fact that an increase in temperature results in a change of water absorptivity (and concentration) as a result of weakening and reduction of hydrogen bonds; water molecules absorb photon energy attributed to the vibrational overtone of the O H bond around 970 nm.[18,60] Therefore, the changes at this wavelength can be considered as a qualitative indicator of water accumulation in the tissue and therefore tissue and cellular edema during heatstroke injury. It is important to note the change occurring in the spectral shape of the absorbance to understand physiological changes during heatstroke. Specifically, we are interested in several wavelengths across the spectra that reflect tissue composition; i.e., characteristic changes in tissue composition at particular wavelengths could be indicative of chromophore behavior. The absorption coefficient of oxyhemoglobin differs from that of deoxyhemoglobin along most of the NIR spectrum.

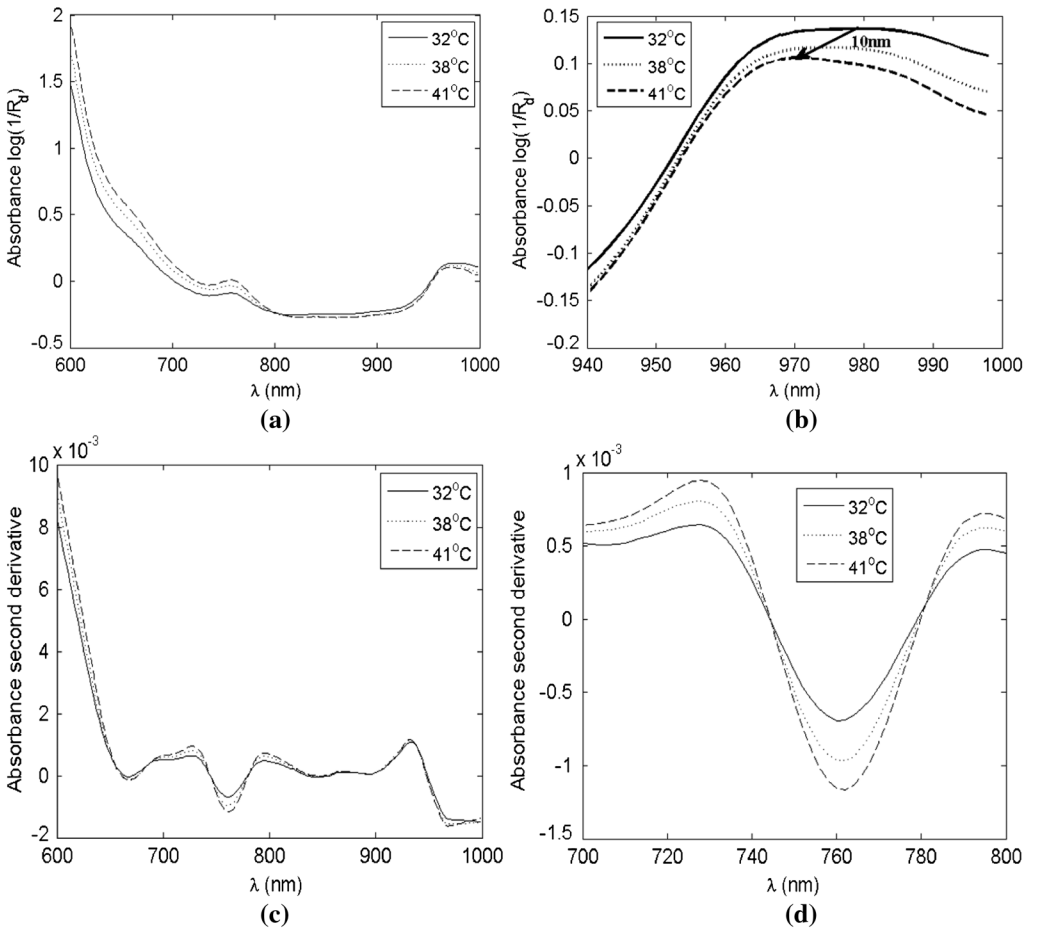

Fig. 2 (a) Representative reflected absorbance (A_s) spectra measured on the brain surface at three different temperatures out of ten using the setup shown in Fig. 1. (b) Enlarged region of Fig. 2(a) between 940 nm $\leq \lambda \leq$ 1000 nm shows the decrease in the intensity peak around 970 nm as the temperature increases. A spectral shift of 10 nm from the baseline to a lower wavelength is demonstrated. (c) Absorbance second-derivative (A_s'') of 2(a). (d) Enlarged region of Fig. 2(c) between 700 nm $\leq \lambda \leq$ 800 nm shows the change in intensity peak around 760 nm as temperature increases.

However, at a certain isosbestic wavelength (~800 nm), the absorption curves cross each other and represent the same value. Thus change in reflectance at an isosbestic wavelength is affected mainly by blood volume (and hence, blood flow) while a change in a non-isosbestic wavelength is affected by the oxy-deoxy ratio as well. The absorbance around 650 nm is mostly affected by the change in deoxyhemoglobin while at 840 nm it is more affected by oxyhemoglobin. Therefore, one can consider the difference between the measurements at different wavelengths as a qualitative representation of the blood oxygenation level. Changes in absorbance intensity spectra confirm our hypothesis that heatstroke causes changes in the optical properties of brain tissue with resultant morphological damage and tissue composition changes. In order to highlight spectral differences that result from an increase in temperature, the spectral second derivative was calculated and is depicted in Fig. 2(c). The spectral region between 700 and 800 nm, magnified in Fig. 2(d), reflects the sensitivity to biochemical (specifically hemoglobin) variations around the center of 760 nm. The changes in absorbance around the isosbestic point (800 nm) suggest that cerebral blood flow is affected following induction of heatstroke. To evaluate the relationship between spectra reflectance and second derivatives versus temperature an exponential function were calculated and depicted in Fig. 3. As can be seen, as the temperature increases the peak reflectance at 970 nm decreases in an exponential fashion as a result of increase in absorption while the peak of the second derivative reflectance at 760 nm increases as a result of hemoglobin variations. We conjecture that heat diffusion to the tissue area may causes hemoglobin denaturation and thereby affect its ability to bind oxygen although the temperature is relatively low. The change in optical absorbance spectra of various hemoglobin species with temperature was also noted in earlier reports.[45,46] Figures 2 and 3 show a consistent pattern among the participant animals throughout this study and confirm our hypothesis that changes in NIR signals can reflect changes in internal temperature in injured brain. Simultaneous measurements of the body physiologic parameters were monitored during heatstroke concurrent to spectral measurements. The variations in heart rate and SpO_2 versus temperature are indicated by the plot in Fig. 4. As shown, an increase in body temperature causes the heart rate to increase and concurrently induce a decrease in oxygen saturation until death. Please note that the SpO_2 is generally above 90% because pulse oximeter measures the saturation of full-oxygenated arterial blood. However, SpO_2 in Fig. 4 is quite low (~75%) even at normal temperature environment. We found that in three mice, the SpO_2 was around 75% while the other two were around 85%. This low SpO_2 maybe the result of oximeter deviation, or/and anesthesia effect. Since the mice are not ventilated, (over) anesthetization can cause respiratory depression

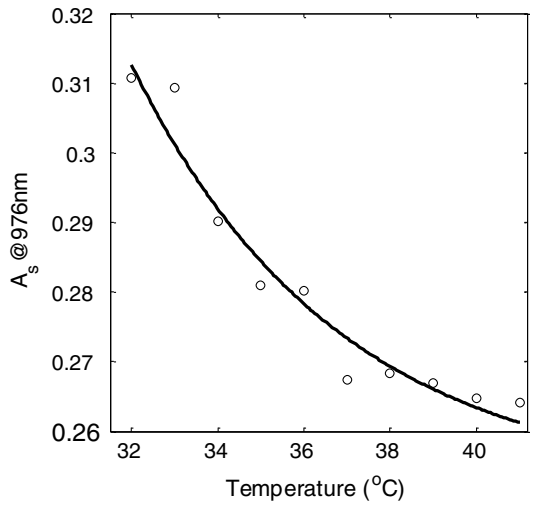

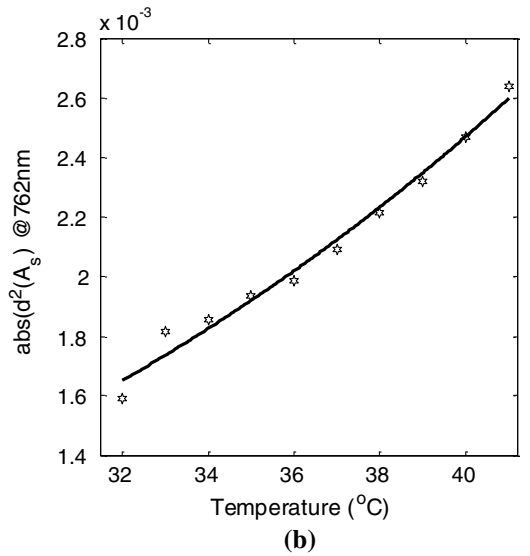

Fig. 3 Absorbance (A_s) and its second derivative (A_s'') intensity at 970 nm and 960 nm, respectively at different temperatures. These results are for the mouse of Fig. 2 and reflect the same trend for the other mice experiments. The points on the graph represent the discrete intensity measurement and the solid line represents the results of exponential fit to this data.

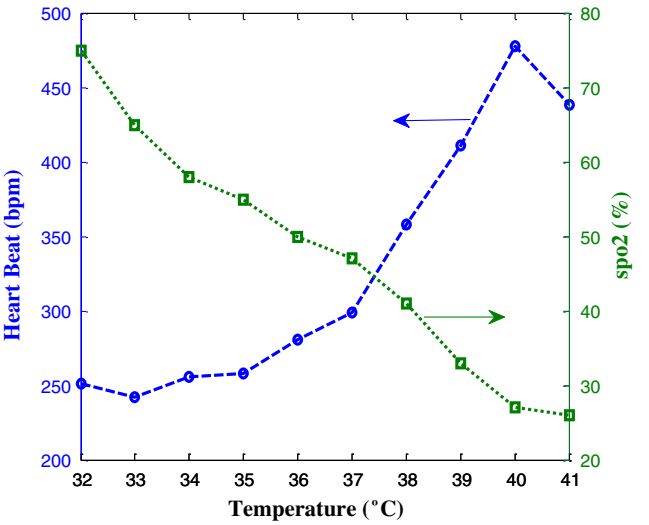

Fig. 4 Graph representation of heart rate (left axis) and SpO_2 (right axis) versus temperature. Solid lines represent spline interpolation between data points. As the temperature increased from 40°C to 41°C the SpO_2 is reversing its increasing trend, a point where the mouse died and heart rate start to decrease.

and low SpO_2. This is very difficult to precisely control in rodent experimental settings.

As seen from Fig. 3, and as we observed along this study, three factors are influenced by increase in temperature: 1. lower reflectance at ~970 nm accompanied by 2. a spectral shift, $\Delta\lambda$, from the baseline temperature and 3. an increase in its second derivative intensity at ~760 nm. These variations motivate us to define a following combined function coined reflectance-temperature index (RTI), which summarizes these significant elements of contrast in a single index. RTI defined as

$$\mathrm{RTI} = \frac{|\ddot{R}_{d@760\ \mathrm{nm}}|}{R_{d@970}} \times \frac{<\lambda>}{\Delta\lambda}. \qquad \text{(dimensionless)} \qquad (5)$$

RTI become more sensitive to temperature elevation as its numerator increase and the denominator strongly decrease causing a total increase in RTI. To bring RTI into a universal index (dimensionless) it was multiply by the average wavelength, $\langle\lambda\rangle$. Since the peak wavelengths which we determine the spectral shift, $\Delta\lambda$, are not sharp but broad [Fig. 2(b)] we calculate the average wavelength, $\langle\lambda\rangle$, from the spectra band where the maximum is. Specifically, to determine $\langle\lambda\rangle$, we scan all the wavelength points where the maximum is and then we calculate the average. For example, in Fig. 2 for the 38°C, we found the maximum at the wavelet's range of 978 to 982 nm. Averaging these five wavelengths results in $\langle\lambda\rangle = 980$ nm. In continuation with Fig. 2, to determine the shift in wavelength as temperature increases ($\Delta\lambda$) we found the maximum absorbance around 970 nm for each temperature and then we calculate the difference between. For example, in Fig. 2 the maxima of the baseline temperature (32°C) found to be at 980 nm while at 38°C it was found to be 970 nm which results in a 10-nm shift. From the entire study we found an average spectral shift from the baseline of $\Delta\lambda = 6.4 \pm 1.93$ nm. The relationship between RTI and temperature derived from Figs. 2 to 3 through an exponential dependence of the form $\mathrm{RTI} = a \times \exp(b \cdot \mathrm{Temp})$ is display in Fig. 5(a) for the above specific mouse. The points on the graph represent the discrete RTI measurement and the solid line represents the results of exponential fit to this data. In Fig. 5(b) a plot of RTI versus temperature data for the entire experiments ($n = 5$) is presented. The data in the graph are the mean and the error bars refer to standard error of positive and negative deviation separately, calculated over each temperature. The solid curve in this figure is the exponential fitting similar to what is shown in Fig. 5(a). As observed, increased temperature leads to a measurable increase in RTI, indicating the feasibility to follow temperature elevation in a non-contact manner using the DRS method. The exponential behavior we observed resembles the exponential increase of intracranial pressure (ICP) during brain injury although further study is necessary to determine the nature of the relationship. The central nervous system is very sensitive to hyperthermia that results in neurologic complications from injury to the cerebellum, basal ganglia, anterior horn cells, and peripheral

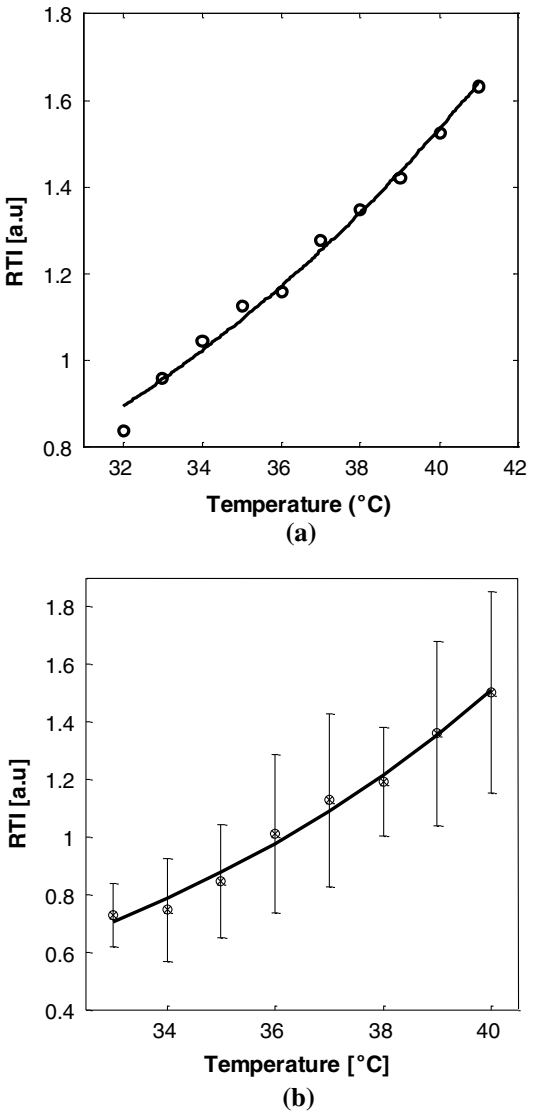

Fig. 5 (a) Plot demonstrating the relationship of the reflectance-temperature index (rTI) to temperature for a single mouse of Fig. 2. As noted, an exponential relationship in the form of $a \cdot \exp(b \times \mathrm{Temp})$ was obtained. Here, $a = 0.00084$, and $b = 0.1$. (b) Graph showing RTI versus of Temperature from the entire experiments ($n = 5$). $\bar{a} = 0.00175 \pm 0.0011$, and $\bar{b} = 0.1143 \pm 0.022$. Data are expressed as mean ± standard error.

nerves. The increase in absorbance at 760 nm (the dominant chromophore being deoxyhemoglobin) with rising body temperature can be explained by two phenomena. First, as a result of cardiopulmonary compromise[61] systemic oxygenation of hemoglobin decreases (as evidenced by decreased oxygen saturation on pulsoximetry in Fig. 4), second, hyperthermic brain injury can result in increased ICP, consistent with previous observations.[62–67] It should be pointed out that no direct assessment of brain function (or dysfunction) was conducted. However, the changes in blood flow (800 nm absorption) provide indirect evidence of altered brain physiology. Neurobehavioral tests were not carried out during this experimental set up due to the terminal (end-point being death) nature of the experiments but can be studied in future nonterminal experiments.

As we show above, the relationship between RTI and temperature can be derived through an exponential dependence of

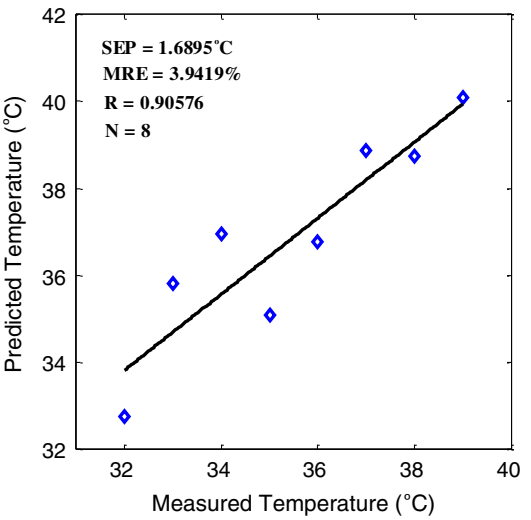

Fig. 6 Comparison between temperatures obtained from Eq. (7) (model predicted) and from the YSI temperature probe measurements. The solid line is the best-fit linear regression fits to the data (open circles). The statistics were obtained from Eq. (5). High correlation between the predicted and actual temperature was obtained with $R = 0.9$ and slope of 0.88.

the form $\mathrm{RTI} = a \times \exp(b \cdot \mathrm{Temp})$. From this expression the temperature can be extracted,

$$\mathrm{Temp} = \frac{1}{b} \times \log\left(\frac{\mathrm{RTI}}{a}\right). \tag{6}$$

To bring this equation to a more general term and based on the entire experiments ($n = 5$), averaged a and b were computed ($\bar{a} = 0.00175 \pm 0.0011$, and $\bar{b} = 0.1143 \pm 0.022$) and Eq. (6) was modified accordingly with $\bar{a}$, $\bar{b}$ instead a, b. Then, the modified Eq. (6) was used back on each of the five mice to predict the temperature and to compare it with the actual temperature. To obtain high correlation fitting, a k-factor was added to the modified equation. Hence,

$$T_{\mathrm{pred}} = \frac{k}{\bar{b}} \times \log\left(\frac{\mathrm{RTI}}{\bar{a}}\right). \tag{7}$$

To demonstrate the possibility of predicting the temperature (T_{pred}) on a new mouse, not included in the previous experiments, we use Eq. (7) and temperature model prediction versus actual temperature is presented in Fig. 6 for the new mouse. A good correlation between prediction to actual temperature was obtained with $R = 0.9$. Inspection of the correlation plots also reveals small RMSE and MRE, respectively. k in this experiment was set to 5.75. The good agreement between the prediction and actual temperature data implies that: 1. RTI can be a candidate marker for temperature assessment during heatstroke and 2. temperature can be monitored noninvasively using the current DRS and Eq. (7). An important point to stress is that Eq. (7) is an empiric mathematical expression and should be studied in future works by increasing the number of animals and comparison with direct brain temperature measurement using conventional probes. This will be the next step in our heatstroke research.

As mentioned previously, optical absorption and scattering coefficients can be extracted with the use of the aforementioned

Eq. (3). Since the diffuse reflectance R_d is measured while ρ, k_1 and k_2 are known parameters we can find the absorption and scattering coefficients by iterating of the both coefficients until the calculated values of the reflection match the measured ones (Levenberg-Marquardt algorithm). It should be pointed out that the increased temperature may affect absorption and absorbance spectra differently since absorbance contains both absorbing effects caused by the chemical components and the scattering effects originated from the structural properties; while the absorption only reflects the chemical absorbing effects on light. The absorption and scattering behavior is illustrated in Fig. 7 at two ranges of temperature; baseline (32°C) and heatstroke (41°C) for the above representative mouse. The points on the graph of Fig. 7(a) represent the discrete calculated absorption coefficient at specific wavelengths and the solid line represents the spline interpolation fit to this data. On the other hand, in Fig. 7(b), the points represents the discrete calculated reduced scattering coefficient at specific wavelengths and the solid line represents the power-law fit to this data. Several studies have shown that the wavelength dependence of scattering in tissue in the NIR obeys a power-law dependence of the form,[68,69]

$$\mu_s'(\lambda) = A\lambda^{-sp}, \tag{8}$$

where $\mu_s' = \mu_s(1-g)$ is the reduced scattering coefficient, g is the anisotropy factor, and μ_s represent the scattering coefficient. A is the scattering amplitude which is related to the density of the scatterers, their distribution, and refractive index changes while sp is the scattering power related to the scatterer size.[70–73] The effect of increased temperature from baseline temperature to heatstroke injury is clearly shown on both panels. From the entire experiments the absorption at 970 and 980 nm was calculated and the averaged absorption was obtained. Results show $\mu_a = 0.015 \pm 0.003$ mm^{-1} at the baseline and $\mu_a = 0.024 \pm 0.007$ mm^{-1} at the heatstroke, which reflects ~37% increase in cerebral tissue absorption following induction of heatstroke. However, one should keep in mind that multiple light scattering can obscure this temperature-water peak if absorption is not separated from the scattering. The change in absorption coefficient is influenced by variation in different tissue biochemical composition such as oxy- and deoxyhemoglobin (650 nm, 830 nm), fat (920 nm), and water (970 nm). This is because optical absorption represents the process of

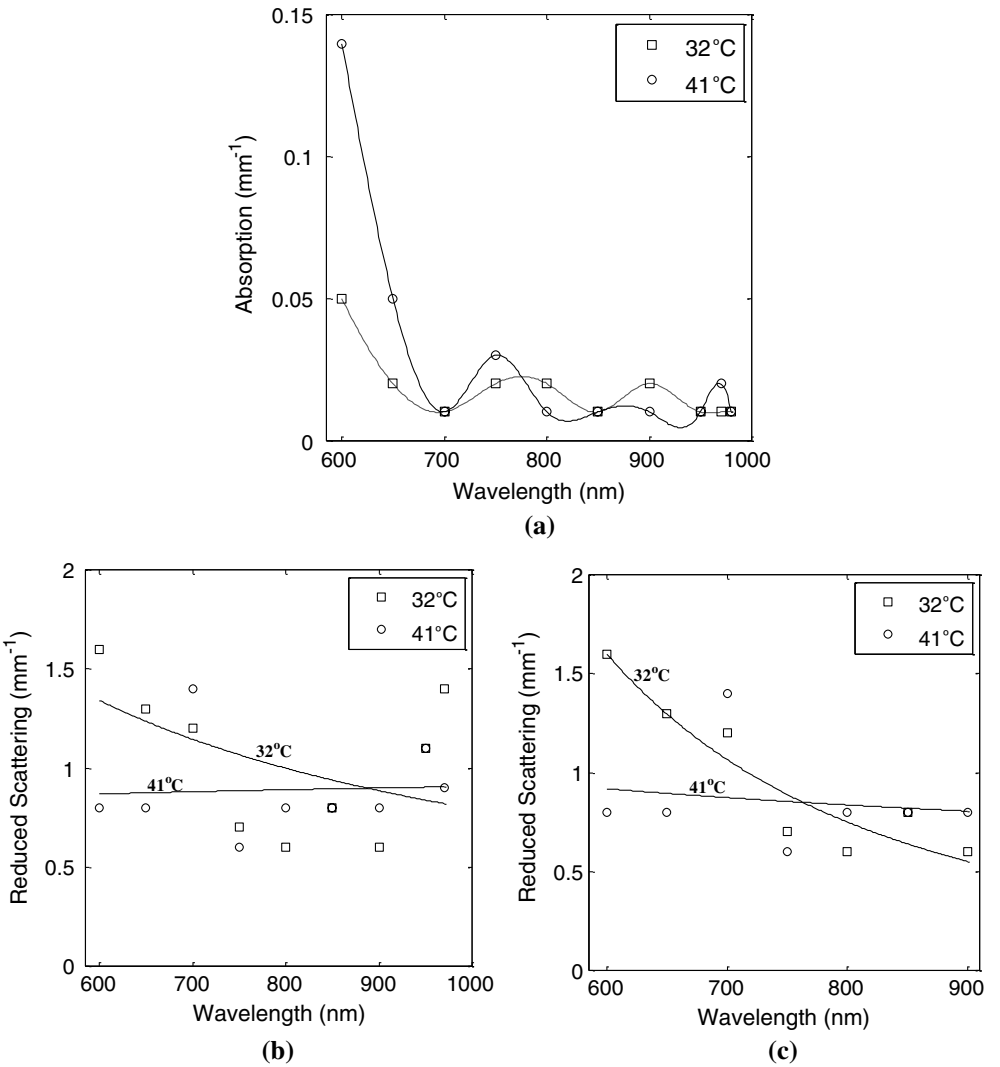

Fig. 7 (a) Absorption, and (b) reduced scattering coefficients obtained by the use of Eq. (3) as a function of temperature for the representative mouse of Fig. 3. The solid line in (a) represent spline interpolation between data points and the solid line in (b) represent the results of power-law fit to this data based on Eq. (7). (c) Improvement in fitting of 7(b) after the last two wavelengths (950 and 970 nm) were taken out.

light attenuation by those chemical components within the brain. On the other hand, analyzing the scattering power show $sp = 1.41 \pm 0.6$ at the baseline and $sp = 0.54 \pm 0.25$ at the heatstroke reflects more than a 60% decrease from the baseline. The change in scattering is attributed to a change in the size and number of scattering particles such as nuclei, mitochondria and protein as well as change in refractive indices (sample inhomogenity); increase in temperature causes severe morphological damage to the tissue, such as denaturation of structural proteins and tissue and cellular edema which in turn affect the scattering properties and thus the light distribution. These morphological changes can be deduced by the slope and amplitude of Fig. 7(b). As can be seen from Fig. 7, while the fitting curve for absorption data is good, the fitting curve for reduced scattering data is quite difficult. This is because the fitting of the scattering is influence greatly from the water peak around 970 nm. Therefore, if we take out the last two wavelengths a better fitting can be achieved as depicted in Fig. 7(c), although data points at 700 nm are far off the curve (may be outliers). Ultimately, these eliminations do not affect our results which show clearly decrease in sp (structural changes). As we move from baseline temperature to heatstroke condition the scattering slope becomes flat, reflecting the increase in particle size or the evolution of swelling of the cells and cell organelle in the brain. Decrease in A reflects the change in the ratio of the refractive index outside (extracellular) to inside (intracellular) the scattering particle. i.e., a drop in A most likely reflects the fact that water changes increases the inhomogeneity of refractive index and thus influence the scattering amplitude. Since during heatstroke the morphological damage in the brain tissue matrix occur which influenced the A and sp parameters, they can therefore serve as a good marker during heatstroke. Overall, changes in both optical properties indicate variation of the pathophysiologic state of the brain and the ability of our setup to follow alteration in temperature during heatstroke over time. The observed change in optical properties versus the temperature is consistent with previous studies that demonstrate that absorption and scattering coefficients can be temperature dependent.[14,17–19,43,74]

4 Conclusion

Heatstroke is an abnormally elevated body temperature with accompanying physical symptoms including changes in the nervous system function. In this work, for the first time to our knowledge, we carried out experimental optical DRS on intact mice brains to a. assess the changes in tissue optical and hemodynamics properties that occurred during heatstroke, and b. to predict internal temperature noninvasively. The measurements were obtained with a single source-detector system orthogonal to each other, and the model of light propagation was employed to recover the optical property coefficients of cerebral tissue from the experimental data. During heatstroke, we note that the intensity peaks of the absorbance at 970 nm and in its second derivative at 760 nm correlate well with increased temperature through an exponential dependence. Reflectance-temperature index (RTI) that reflects changes in reflectance intensity and spectral shift from baseline was derived from DRS data. That is, we used the difference in spectra properties through RTI to estimate the influence of temperature on the internal rodent brain tissue. Although our pilot measurements are preliminary, results from a mouse show that RTI can be a good predictor for temperature measurement ($R = 0.9$). It should be pointed out that the ability to determine the calibration factor k in Eq. (6) is to have a complete dataset for calibration containing different temperature levels expected to be encountered during routine analysis. However, this can be accomplished during the calibration process with a dataset that is well representative changes in temperature conditions. Our future work will focus on further testing of the system on more mice and the applicability of Eq. (6) and applying appropriate calibration/validation modeling such as partial-least square (PLS) regression.[12] We also report the change in cerebral optical properties, based on the use of diffusion model, which reflects the variation in chromophores content and brain structure during heatstroke. The reported technique is simple, inexpensive, easy to implement, and can therefore be adapted in the future for temperature monitoring in clinical and laboratory settings as well.

Acknowledgments

Authors would like to gratefully acknowledge the anonymous reviewers' for all their valuable comments and useful suggestions making the manuscript clearer and more focused. D. Abookasis also gratefully acknowledges both Ariel University and the Israeli Ministry of Absorption's for their support as part of the "returning scientists" program.

References

1. A. Bouchama and J. P. Knochel, "Heat stroke," *N. Engl. J. Med.* **346**(25), 1978–1988 (2002).
2. H. B. Simon, "Hyperthermia," *N. Engl. J. Med.* **329**(7), 483–487 (1993).
3. D. M. Hall et al., "Mechanisms of circulatory and intestinal barrier dysfunction during whole body hyperthermia," *Am. J. Physiol. Heart. Circ. Physiol.* **280**(2), H509–H521 (2001).
4. J. Kalita and U. K. Misra, "Neurophysiological studies in a patient with heat stroke," *Neurology* **248**(11), 993–995 (2001).
5. M. G. Austin and J. W. Berry, "Observation of one hundred cases of heatstroke," *J. Am. Med. Assoc.* **161**(16), 1525–1529 (1956).
6. Y. Shapiro and D. S. Seidman, "Field and clinical observations of exertional heat stroke patients," *Med. Sci. Sports. Exerc.* **22**(1), 6–14 (1990).
7. A. Bouchama et al., "Ineffectiveness of dantrolene sodium in the treatment of heatstroke," *Crit. Care. Med.* **19**(2), 176–180 (1991).
8. R. T. Pettigrew et al., "Circulatory and biochemical effects of whole body hyperthermia," *Br. J. Surg.* **61**(9), 727–730 (1974).
9. C. H. Wyndham, N. B. Strydom, and H. M. Cooke, "Methods of cooling subjects with hyperpyrexia," *J. Appl. Physiol.* **14**(5), 771–776 (1959).
10. E. Hadad et al., "Heat stroke, a review of cooling methods," *Sports. Med.* **34**(8), 501–511 (2004).
11. A. Bouchama, M. Dehbi, and E. Chaves-Carballo, "Cooling and hemodynamic management in heatstroke: practical recommendations," *Crit. Care.* **11**(3), R54 (2007).
12. V. S. Hollis, Chapter 4, *Non-Invasive Monitoring of Brain Tissue Temperature by Near-Infrared Spectroscopy*, PhD Dissertation, University of London (2002).
13. A. N. Amini, E. S. Ebbini, and T. T. Georgiou, "Noninvasive estimation of tissue temperature via high-resolution spectral analysis techniques," *IEEE. Trans. Bio. Eng.* **52**(5), 221–228 (2005).
14. V. Tuchin, *Tissue Optics: Light Scattering Methods and Instruments for Medical Diagnosis*, 2nd ed., SPIE Press, Bellingham, WA (2007).
15. L. V. Wang and H-i. Wu, *Biomedical Optics: Principles and Imaging*, John Wiley & Sons, Inc., Hoboken, New Jersey (2007).
16. D. A. Boas, C. Pitris, and N. Ramanujam, *Handbook of Biomedical Optics*, CRC Press, Boca Raton, Florida (2011).
17. N. Kakuta et al., "Temperature measurements of turbid aqueous solutions using near-infrared spectroscopy," *Appl. Opt.* **47**(13), 2227–2233 (2008).
18. S. H. Chung et al., "Non-invasive tissue temperaure measurements based on quantitative diffuse optical spectroscopy (DOS) of water," *Phys. Med. Biol.* **55**(13), 3753–3765 (2010).

19. J. Laufer et al., "Effect of temperature on the optical properties of *ex vivo* human dermis and subdermis," *Phys. Med. Biol.* **43**(9), 2479–2489 (1998).
20. M. Sato et al., "*In vivo* rat brain measurements of changes in signal intensity depth profiles as a function of temperature using wide-field optical coherence tomography," *Appl. Opt.* **49**(30), 5686–5696 (2010).
21. M. Li et al., "Functional laser speckle imaging of cerebral blood flow under hypothermia," *J. Biomed. Opt.* **16**(8), 086011 (2011).
22. J. Lin and C. W. Brown, "Near-IR fiber-optic temperature sensor," *Appl. Spect.* **47**(1), 62–68 (1993).
23. K. Vishwanath et al., "Portable, fiber-based, diffuse reflection spectroscopy (DRS) systems for estimating tissue optical properties," *Appl. Spect.* **65**(2), 206–215 (2011).
24. M. G. Nichols, E. L. Hull, and T. H. Foster, "Design and testing of a white-light, steady-state diffuse reflectance spectrometer for determination of optical properties of highly scattering systems," *Appl. Opt.* **36**(1), 93–104 (1997).
25. R. J. Mallia et al., "Diffuse reflection spectroscopy: an alternative to autofluorescence spectroscopy in tongue cancer detection," *Appl. Spect.* **64**(4), 409–418 (2010).
26. G. Zonios et al., "Diffuse reflectance spectroscopy of human adenomatous colon polyps *in vivo*," *Appl. Opt.* **38**(31), 6628–6637 (1999).
27. E. Hull and T. Foster, "Steady-state reflectance spectroscopy in the P3 approximation," *J. Opt. Soc. Am. A* **18**(3), 584–599 (2001).
28. Y. N. Mirabal et al., "Reflectance spectroscopy for in vivo detection of cervical precancer," *J. Biomed. Opt.* **7**(4), 587–594 (2002).
29. D. T. Delpy et al., "Estimation of optical pathlength through tissue from direct time of flight measurement," *Phys. Med. Biol.* **33**(12), 1433–1442 (1988).
30. M. Cope, "The Development of a Near-Infrared spectroscopy system and its application for noninvasive monitoring of cerebral blood and tissue oxygenation in the newborn infant," Ph.D. Dissertation, University College London, London (1991).
31. H. Liu et al., "Determination of optical properties and blood oxygenation in tissue using continuous NIR light," *Phys. Med. Biol.* **40**(11), 1983–1993 (1995).
32. G. Kumar and J. M. Schmitt, "Optimal probe geometry for near-infrared spectroscopy of biological tissue," *Appl. Opt.* **36**(10), 2286–2293 (1997).
33. S. C. Kanick, H. J. C. M. Sterenborg, and A. Amelink, "Empirical model of the photon path length for a single fiber reflectance spectroscopy device," *Opt. Express* **17**(2), 860–871 (2009).
34. R. M. P. Doornbos et al., "The determination of *in vivo* human tissue optical properties and absolute chromophore concentrations using spatially resolved steady-state diffuse reflectance spectroscopy," *Phys. Med. Biol.* **44**(4), 967–982 (1999).
35. J. M. Schmitt and G. Kumar, "Optical scattering properties of soft tissue: a discrete particle model," *Appl. Opt.* **37**(13), 2788–2797 (1998).
36. R. L. P. van Veen et al., "Optical biopsy of breast tissue using differential path-length spectroscopy," *Phys. Med. Biol.* **50**(11), 2573–2581 (2005).
37. J. C. Finlay and T. H. Foster, "Hemoglobin oxygen saturations in phantoms and *in vivo* from measurements of steady-state diffuse reflectance at a single, short source-detector separation," *Med. Phys.* **31**(7), 1949–1959 (2004).
38. T-Y. Tseng et al., "Quantification of the optical properties of two-layered turbid media by simultaneously analyzing the spectral and spatial information of steady-state diffuse reflectance spectroscopy," *Biomed. Express* **2**(4), 901–914 (2011).
39. F. Bevilacqua et al., "Broadband absorption spectroscopy in turbid media by combined frequency-domain and steady-state methods," *Appl. Opt.* **39**(34), 6498–6507 (2000).
40. T. J. Farrell, M. S. Patterson, and B. Wilson, "A diffusion theory model of spatially resolved, steady-state diffuse reflectance for the noninvasive determination of tissue optical properties *in vivo*," *Med. Phys.* **19**(4), 879–888 (1992).
41. S. H. Chung et al., "Non-invasive measurement of deep tissue temperature changes caused by apoptosis during breast cancer neoadjuvant chemotherapy: a case study," *J. Innov. Opt. Health. Sci.* **4**(4), 361–372 (2011).
42. F. J. van der Meer et al., "Temperature-dependent optical properties of individual vascular wall components measured by optical coherence tomography," *J. Biomed. Opt.* **11**(4), 041120 (2006).
43. R. Agah et al., "Dynamics of temperature dependent optical properties of tissue: dependence on thermally induced alteration," *IEEE. Trans. Biomed. Eng.* **43**(8), 839–846 (1996).
44. B. Cletus et al., "Temperature-dependent optical properties of Intralipid® measured with frequency-domain photon-migration spectroscopy," *J. Biomed. Opt.* **15**(1), 017003 (2010).
45. J. M. Steinke and A. P. Shepherd, "Effects of temperature on optical absorbance spectra of oxy-, carboxy-, and deoxyhemoglobin," *Clin. Chem.* **38**(7), 1360–1364 (1992).
46. L. Cordone et al., "Optical absorption spectra of deoxy- and oxyhemoglobin in the temperature range 300-20–K. Relation with protein dynamics," *Biophys. Chem.* **24**(3), 259–275 (1986).
47. K. H. Hazen, M. A. Arnold, and G. W. Small, "Temperature-Insensitive Near-Infrared Spectroscopic Measurement of Glucose in Aqueous Solutions," *Appl. Spect.* **48**(4), 477–483 (1994).
48. P. S. Jensen, J. Bak, and S. Andersson-Engels, "Influence of temperature on water and aqueous glucose absorption spectra in the near- and mid-infrared regions at physiologically relevant temperatures," *Appl. Spect.* **57**(1), 28–36 (2003).
49. M. J. Haller et al., "Adverse impact of temperature and humidity on blood glucose monitoring reliability: a pilot study," *Diab. Tech. Ther.* **9**(1), 1–9 (2007).
50. R. Liu et al., "Influence of temperature on the precision of noninvasive glucose sensing by near-infrared spectroscopy," *Proc. SPIE* **6863**, 68630Q (2008).
51. Z. A. Damanhouri and O. S. Tayeb, "Animal models for heat stroke studies," *J. Pharmacol. Toxicol. Methods* **28**(3), 119–127 (1992).
52. R. V. Maikala, "Modified Beer's Law—historical perspectives and relevance in near-infrared monitoring of optical properties of human tissue," *J. Indust. Ergon.* **40**(2), 125–134 (2010).
53. A. Ishimaru, *Wave Propagation and Scattering in Random Media*, Academic Press, New York (1978).
54. J. L. Karagiannes et al., "Applications of the 1-D diffusion approximation to the optics of tissues and tissue phantoms," *Appl. Opt.* **28**(12), 2311–2317 (1989).
55. R. C. Haskell et al., "Boundary conditions for the diffusion equation in radiative transfer," *J. Opt. Soc. Am. A* **11**(10), 2727–2741 (1994).
56. K. Yoo, F. Liu, and R. Alfano, "When does the diffusion-approximation fail to describe photon transport in random-media," *Phys. Rev. Lett.* **64**(22), 2647–2650 (1990).
57. A. D. Kim and A. Ishimaru, "Optical diffusion of continuous-wave, pulsed and density waves in scattering media and comparisons with radiative transfer," *Appl. Opt.* **37**(22), 5313–5319 (1998).
58. S. Fantini, M. A. Franceschini, and E. Gratton, "Semi-infinite-geometry boundary problem for light migration in highly scattering media: a frequency-domain study in the diffusion approximation," *J. Opt. Soc. Am. B* **11**(10), 2128–2138 (1994).
59. M. Riedl, *Optical Design Fundamentals for Infrared Systems*, 2nd ed., SPIE Press, Bellingham, WA (2001).
60. J. Workman and L. Weyer, *Practical Guide to Interpretive Near-Infrared Spectroscopy*, CRC Press, Boca Raton, FL (2008).
61. G. M. Eshel and P. Safar, "The role of the central nervous system in heatstroke: reversible profound depression of cerebral activity in a primate model," *Aviat. Space. Environ. Med.* **73**(4), 327–332 (2002).
62. C. J. Shih, M. T. Lin, and S. H. Tsai, "Experimental study on the pathogenesis of heat stroke," *J. Neurosurg.* **60**(6), 1246–52 (1984).
63. M.-T. Lin, C.-P. Chang, and S.-H. Chen, "The Efficacy of Opioid Antagonists Against Heatstroke-Induced Ischemia and Injury in Rats," Chapter 33, in *Opiate Receptors and Antagonists: From Bench to Clinic*, R. Dean, E. J. Bilsky, and S. S. Negus, Ed., Humana Press, New York (2009).
64. M.-T. Lin et al., "Interleukin-1β production during the onset of heat stroke in rabbits," *Neurosci. Lett.* **174**(1), 17–20 (1994).
65. C. T. McLaughlina, A. G. Kaneb, and A. E. Auberc, "MR Imaging of heat stroke: external capsule and thalamic t1 shortening and cerebellar injury," *J. Am. Neurorad.* **24**(7), 1372–1375 (2003).
66. C. -K. Chang et al., "Effect of hypervolaemic haemodilution on cerebral glutamate, glycerol, lactate and free radicals in heatstroke rats," *Clin. Sci.* **106**(5), 501–509 (2004).
67. M. T. Lin and S. Z. Lin, "Cerebral ischemia is the main cause for the onset of heat stroke syndrome in rabbits," *Cell. Mol. Sci.* **48**(3), 225–227 (1992).
68. H. J. Van Staveren et al., "Light scattering in Intralipid-10% in the wavelength range of 400–1100 nm," *Appl. Opt.* **30**(31), 4507–4514 (1991).

69. R. Graaff et al., "Reduced light-scattering properties for mixtures of spherical particles: a simple approximation derived from Mie calculations," *Appl. Opt.* **31**(10), 1370–1376 (1992).
70. J. R. Mourant et al., "Predictions and measurements of scattering and absorption over broad wavelength ranges in tissue phantoms," *Appl. Opt.* **36**(4), 949–957 (1997).
71. A. M. K. Nilsson et al., "Changes in spectral shape of tissue optical properties in conjunction with laser-induced thermotherapy," *Appl. Opt.* **37**(7), 1256–1267 (1998).
72. C. Lau et al., "Re-evaluation of model-based light-scattering spectroscopy for tissue spectroscopy," *J. Biomed. Opt.* **14**(2), 024031 (2009).
73. X. Wang et al., "Approximation of Mie scattering parameters in near-infrared tomography of normal breast tissue *in vivo*," *J. Biom. Opt.* **10** (5), 051704 (2005).
74. V. V. Tuchin, *Handbook of Optical Biomedical Diagnostics*, SPIE Press, Bellingham, WA (2002).